models. High TEER was observed in the models constructed with pericytes, as compared with those without pericytes. In addition, endothelial cells in contact with pericytes (EP0, EPA) showed higher TEER than those out of contact with pericytes (E0P, EAP).

The paracellular permeability of RBEC monolayers measured by the water soluble small marker fluorescein was the highest in endothelial mono-cultures, indicating the leakiest barrier (Fig. 3). The presence of astrocytes or pericytes in either double or triple co-culture systems significantly decreased the flux of the tracer. In double co-culture models the in-contact types EA0 and EP0 showed lower permeability for Na-F than the non-contact types E0A and E0P (Fig. 3).

Our results on pericytic induction of BBB properties are in agreement with recent publications. Rat pericytes could decrease the paracellular permeability and enhance *P*-glycoprotein activity in a mouse brain endothelial cell line, MBEC4 (Dohgu et al. 2005). The mRNA expression of MRP6 efflux pump was also up-regulated in bovine brain endothelial cells by pericytes (Berezowski et al. 2004). Some of the factors mediating this effect have been identified. The upregulation of BBB properties in MBEC4 cells was induced by transforming growth factor-β production in pericytes (Dohgu et al. 2005). Pericyte-derived angiopoietin-1 enhanced occludin gene expression in a brain endothelial cell line (Hori et al. 2004). Moreover, extracellular matrix from pericytes improved the tightness of porcine cerebral endothelial cells (Hartmann et al. 2007).

The triple BBB models published earlier used combinations of brain endothelial cells, astrocytes and neurons. The presence of both astrocytes and neurons decreased the paracellular permeability of RBE4 immortalized rat brain endothelial cells (Schiera et al. 2005). In a flow-based in vitro BBB model, the differentiation of serotonergic neurons was promoted by the endothelial-glial co-culture (Stanness et al. 1999). Although EPA is not the first BBB model using three cell types, this is the first rat primary culture-based syngeneic model that uses brain pericytes.

These results clearly confirm that cellular communications play an important role in inducing and maintaining the barrier function of brain endothelial cells. Brain endothelial cells without the influence of astrocytes or pericytes showed the weakest barrier tightness, indicating the loss of BBB properties in culture conditions in the absence of cellular cross-talk.

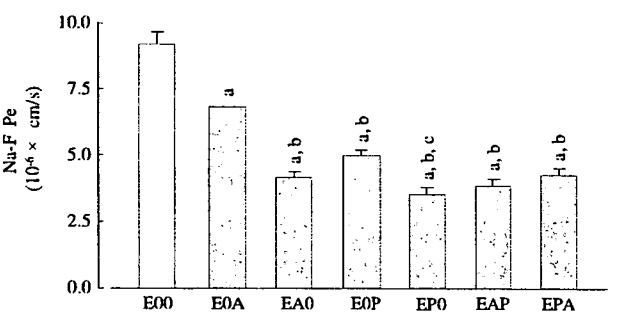

Fig. 3 Transendothelial permeability (Pe) changes for paracellular permeability marker sodium fluorescein (Na-F) in brain capillary endothelial cell monolayers of in vitro BBB models. Results (10^{-6} cm/s) are presented as means ± SEM. $n = 4$. $^{a}P < 0.01$ was considered statistically significant difference in the P_e, as compared to E00, $^{b}P < 0.01$ to E0A, and $^{c}P < 0.05$ to E0P, respectively

The major finding of the experiments is that brain microvessel pericytes are able to strengthen the BBB function of endothelial cells, like astrocytes, widely used in BBB models. Pericytes could induce a tighter barrier than astrocytes. The in-contact models were tighter than the out-of-contact types, and triple models showed better barrier properties than double co-cultures. As brain endothelial cells, pericytes and astrocytes, composing the brain microvasculature, have their own roles at the BBB, the EPA co-culture system constructed with all three types of cells seems to be a promising new in vitro BBB model.

Acknowledgments The work was partly supported by Grants for New Industry Creative-Type Technology R&D promotion Programs from the Ministry of Economy, Trade and Industry (2005, 2006), Grant-In-Aid for Scientific Research from the Ministry Education, Culture, Sports, Science and Technology, Japan, and Grants from the Hungarian Research Fund (OTKA T37834) and National Office for Research and Technology (RET 08/2004).

References

Abbott NJ (2005) Dynamics of CNS barriers: evolution, differentiation, and modulation. Cell Mol Neurobiol 25:5–23

Abbott NJ, Ronnback L, Hannson E (2006) Astrocyte-endothelial interactions at the blood–brain barrier. Nat Rev Neurosci 7:41–53

Berezowski V, Landry C, Dehouck M-P, Cecchelli R, Fenart L (2004) Contribution of glial cells and pericytes to the mRNA profiles of P-glycoprotein and multidrug resistance-associated proteins in an in vitro model of the blood-brain barrier. Brain Res 1018:1–9

Deli MA, Szabó CA, Dung NTK, Joó F (1997) Immunohistochemical and electron microscopy detections on primary cultures of rat cerebral endothelial cells. In: Boer AG, Sutanto W (eds) Drug transport across the blood–brain barrier: in vivo and in vitro techniques. Harwood Academic Publishers, Amsterdam, pp 23–28

Deli MA, Ábrahám CS, Kataoka Y, Niwa M (2005) Permeability studies on in vitro blood-brain barrier models: physiology, pathology, and pharmacology. Cell Mol Neurobiol 25:59–127

Dohgu S, Takata F, Yamauchi A, Nakagawa S, Egawa T, Naito M, Tsuruo T, Sawada Y, Niwa M, Kataoka Y (2005) Brain pericytes contribute to the induction and up-regulation of blood–brain barrier functions through transforming growth factor-beta production. Brain Res 1038:208–215

Hartmann C, Zozulya A, Wegener J, Galla HJ (2007) The impact of glia-derived extracellular matrices on the barrier function of cerebral endothelial cells: an in vitro study. Exp Cell Res 313:1318–1325

Haseloff RF, Blasig IE, Bauer H-C, Bauer H (2005). In search of the astrocytic factor(s) modulating blood–brain barrier functions in brain capillary endothelial cells in vitro. Cell Mol Neurobiol 25:25–39

Hayashi K, Nakao S, Nakaoke R, Nakagawa S, Kitagawa N, Niwa M (2004) Effects of hypoxia on endothelial/pericytic co-culture model of the blood–brain barrier. Regul Pept 123:77–83

Hellström M, Gerhardt H, Kalén M, Li X, Eriksson U, Wolburg H, Betsholtz C (2001) Lack of pericytes leads to endothelial hyperplasia and abnormal vascular morphogenesis. J Cell Biol 153:543–553

Hoheisel D, Nitz T, Franke H, Wegener J, Hakvoort A, Tilling T, Galla HJ (1998) Hydrocortisone reinforces the blood–brain barrier properties in a serum free cell culture system. Biochem Biophys Res Commun 247:312–315

Hori S, Ohtsuki S, Hosoya K, Nakashima E, Terasaki T (2004) A pericyte-derived angiopoietin-1 multimeric complex induces occludin gene expression in brain capillary endothelial cells through Tie-2 activation in vitro. J Neurochem 89:503–513

Joó F (1996) Endothelial cells of the brain and other organ systems: some similarities and differences. Prog Neurobiol 48:255–273

Kis B, Deli MA, Kobayashi H, Ábrahám CS, Yanagita T, Kaiya H, Isse T, Nishi R, Gotoh S, Kangawa K, Wada A, Greenwood J, Niwa M, Yamashita H, Ueta Y (2001) Adrenomedullin regulates blood–brain barrier functions in vitro. Neuroreport 12:4139–4142

Perrière N, Demeuse P, Garcia E, Regina A, Debray M, Andreux J-P, Couvreur P, Schermann J-M, Temsamani J, Couraud P-O, Deli MA, Roux F (2005) Puromycin-based purification of rat brain capillary endothelial cell cultures. Effect on the expression of blood-brain barrier-specific properties. J Neurochem 93:279–289

Schiera G, Sala S, Gallo A, Raffa MP, Pitarresi GL, Savettieri G, Di Liegro I (2005) Permeability properties of a three-cell type in vitro model of blood-brain barrier. J Cell Mol Med 9:373–379

Stanness KA, Neumaier JF, Sexton TJ, Grant GA, Emmi A, Maris DO, Janigro D (1999) A new model of the blood–brain barrier: co-culture of neuronal, endothelial and glial cells under dynamic conditions. Neuroreport 10:3725–3731

Tao-Cheng JH, Nagy Z, Brightman MW (1987) Tight junctions of brain endothelium in vitro are enhanced by astroglia. J Neurosci 7:3293–3299

Hot spots in prion protein for pathogenic conversion

Kazuo Kuwata[†‡§], Noriyuki Nishida[¶], Tomoharu Matsumoto[†], Yuji O. Kamatari[†], Junji Hosokawa-Muto[†], Kota Kodama[†], Hironori K. Nakamura[†], Kiminori Kimura[†], Makoto Kawasaki[¶], Yuka Takakura[¶], Susumu Shirabe[‖], Jiro Takata[††], Yasufumi Kataoka[††], and Shigeru Katamine[¶]

[†]Center for Emerging Infectious Diseases, [‡]Department of Gene and Development, Graduate School of Medicine, Gifu University, 1-1 Yanagido, Gifu 501-1194, Japan; [¶]Department of Molecular Microbiology and Immunology, [‖]Internal Medicine I, Nagasaki University Graduate School of Biomedical Sciences, 1-12-4 Sakamoto, Nagasaki 852-8523, Japan; and [††]Department of Pharmaceutical Care and Health Sciences, Faculty of Pharmaceutical Sciences, Fukuoka University, 8-19-1 Nanakuma, Jyonann-ku, Fukuoka 814-0180, Japan

Edited by Stanley B. Prusiner, University of California, San Francisco, CA, and approved June 6, 2007 (received for review March 22, 2007)

Prion proteins are key molecules in transmissible spongiform encephalopathies (TSEs), but the precise mechanism of the conversion from the cellular form (PrP^C) to the scrapie form (PrP^{Sc}) is still unknown. Here we discovered a chemical chaperone to stabilize the PrP^C conformation and identified the hot spots to stop the pathogenic conversion. We conducted *in silico* screening to find compounds that fitted into a "pocket" created by residues undergoing the conformational rearrangements between the native and the sparsely populated high-energy states (PrP*) and that directly bind to those residues. Forty-four selected compounds were tested in a TSE-infected cell culture model, among which one, 2-pyrrolidin-1-yl-*N*-[4-[4-(2-pyrrolidin-1-yl-acetylamino)-benzyl]-phenyl]-acetamide, termed GN8, efficiently reduced PrP^{Sc}. Subsequently, administration of GN8 was found to prolong the survival of TSE-infected mice. Heteronuclear NMR and computer simulation showed that the specific binding sites are the A-S2 loop (N159) and the region from helix B (V189, T192, and K194) to B-C loop (E196), indicating that the intercalation of these distant regions (hot spots) hampers the pathogenic conversion process. Dynamics-based drug discovery strategy, demonstrated here focusing on the hot spots of PrP^C, will open the way to the development of novel anti-prion drugs.

anti-prion compound | binding sites | chemical chaperone | dynamics-based drug discovery | transmissible spongiform encephalopathy

The accumulation of abnormal protease-resistant prion protein (PrP^{Sc}), a conformational isoform of cellular prion protein (PrP^C), is a key event in the pathogenesis of transmissible spongiform encephalopathies (TSEs) (1–3), and this host-encoded PrP^C has a crucial role in the development of the diseases (4, 5). Because details of the mechanism of conversion from PrP^C to PrP^{Sc} still remain obscure at this stage, PrP^C could be an appropriate molecular target for the drug treatment of TSEs (6) for avoiding the problems associated with the strain differences in PrP^{Sc} (7). PrP^C is a membrane-anchored glycosylated protein and is well conserved in mammals, and its physiological function is currently argued (8). The three-dimensional structure of recombinant PrP^C has been elucidated by NMR (9–13). Briefly, it contains a globular fold with three α-helices (A, B, and C) and a small, imperfectly formed β-sheet (S1 and S2).

The pathogenic conversion process could be related to the thermal stability or the global conformational fluctuation of PrP^C. Recently, a metastable state of the PrP^C was characterized by using a high-pressure NMR (14), where hydrostatic pressure was elevated up to 2,500 bar in an on-line high-pressure NMR cell. The thermodynamical stability profile shows that diverse residues in helices B and C are less stable, indicating the formation of the intermediate conformation (PrP*) (14). Subsequently, a Carr–Purcell–Meiboom–Gill relaxation–dispersion study revealed that slow fluctuation on a time scale of microseconds to milliseconds occurs at the corresponding regions [supporting information (SI) Fig. 4*a*], indicating the conformational rearrangements occurring between the native and the sparsely populated high-energy states (15, 16). Interestingly, mutations related to familial forms of the prion diseases are rather concentrated in helices B and C (SI Fig. 4*b*), and their distribution is somewhat similar to that of slowly fluctuating regions. Moreover, those residues form a major cavity (Fig. 1*a*, green). Thus, a small substance capable of specifically binding to those residues could stabilize the PrP^C conformation because of the decrease in the Gibbs free energy of PrP^C upon binding (6), as well as the suppression of the conformational rearrangements by cross-linking of distant regions. We termed this strategy dynamics-based drug discovery. Because PrP^{Sc} is gradually degraded in *ex vivo* experiments (17, 18), such a population shift toward PrP^C will result in a decrease in PrP^{Sc} population.

Based on dynamics-based drug discovery, we conducted a search for chemical compounds that could specifically bind to the unstable residues. We focused on 14 amino acid residues (M129, G131, N159, V161, Y162, D178, C179, T183, I184, L185, H187, T190, G195, and E196, shown in red with side chain in Fig. 1*a*), located in the loop between helix A and S2 (A-S2 loop) and the loop between helices B and C (B-C loop). A virtual ligand screening program initially picked up 624 chemicals potentially capable of binding to the pocket (Fig. 1*a*, green) with a binding score better (i.e., less) than −32 (SI Table 1), of 320,000 candidates in a database. We further selected the compounds that formed hydrogen bonds with at least one of the 14 amino acids. With careful examination of binding modes, taking into account Lipinski's rules (19), we then selected the 59 compounds showing the lowest predicted binding free energy.

Results

To evaluate the effect of the selected compounds on the conversion of PrP, we next conducted *ex vivo* screening. We used a mouse neuronal cell culture uninfected (GT1-7) and persistently infected with human TSE agent (Fukuoka-1 strain), designated GT+FK (20). Of the 59 compounds, we tested the 44 that were commercially available (see SI Table 1). Among these, 2-pyrrolidin-1-yl-*N*-[4-[4-(2-pyrrolidin-1-yl-acetylamino)-benzyl]-phenyl]-acetamide (compound number 8, molecular weight 420) (Fig. 1*b*) was found to significantly inhibit the PrP^{Sc}

Author contributions: K. Kuwata designed research; K. Kuwata, N.N., T.M., Y.O.K., J.H.-M., K. Kodama, H.K.N., K. Kimura, M.K., Y.T., S.S., J.T., Y.K., and S.K. performed research; H.K.N. analyzed data; K. Kuwata wrote the paper; K. Kuwata performed the NMR measurements and *in silico* screening; N.N. and J.H.-M. performed the *ex vivo* and *in vivo* screening; T.M. prepared the labeled and nonlabeled recombinant PrP; Y.O.K. measured NMR spectra; K. Kodama synthesized GN8; K. Kimura, M.K., Y.T., S.S., and S.K. were mainly engaged in the *in vivo* experiment; and J.T. and Y.K. prepared GN8 aqueous solution for injection and the *in vivo* test.

The authors declare no conflict of interest.

This article is a PNAS Direct Submission.

Abbreviations: TSE, transmissible spongiform encephalopathy; PrP, prion protein; PrP^C, cellular isoform of PrP; PrP^{Sc}, scrapie isoform of PrP; PrP*, sparsely populated high-energy state of PrP; BSE, bovine spongiform encephalopathy; d.p.i., days postinoculation.

[§]To whom correspondence should be addressed. E-mail: kuwata@gifu-u.ac.jp.

This article contains supporting information online at www.pnas.org/cgi/content/full/0702671104/DC1.

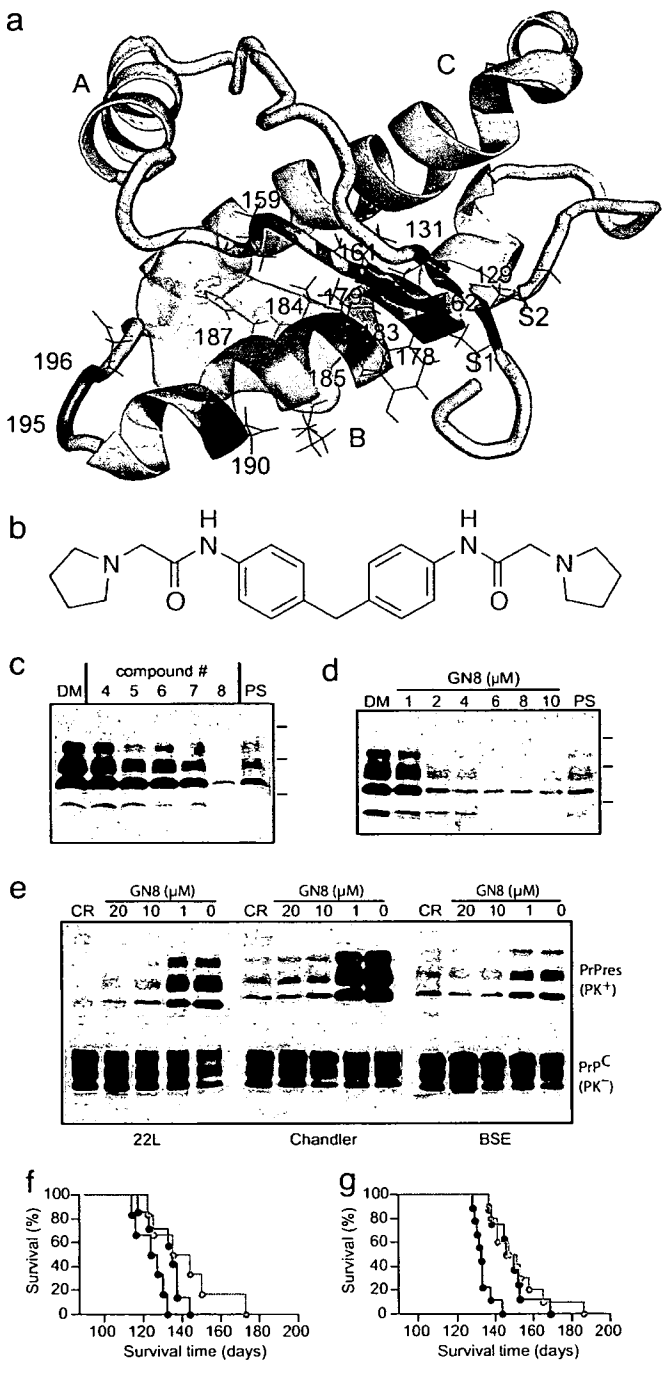

Fig. 1. *In silico* and *ex vivo* screening. (*a*) Residues undergoing global fluctuation displayed as a wire frame in red mapped on the mouse PrP^C structure (residues 124–226) (12), and a binding pocket defined by those residues, colored green. S1, A, S2, B, and C indicate S1 strand, helix A, S2 strand, helix B, and helix C, respectively. The image was created by using PyMol (www.pymol.org). (*b*) 2-Pyrrolidin-1-yl-*N*-[4-[4-(2-pyrrolidin-1-yl-acetylamino)-benzyl]-phenyl]-acetamide, termed GN8. (*c*) Western blotting of PrP^{Sc} in GT+FK cells after treatment with different compounds picked up by *in silico* screening. The cells treated with no. 8 compound showed significant reduction of PrP^{Sc}, which was better than that with 10 μg/ml pentosan polysulfate. DM, DMSO at 0.1%; PS, 10 μg/ml pentosan polysulfate. Molecular masses (37, 25, and 15 kDa) are indicated by bars on the right side of the panels. (*d*) PrP^{Sc} signals in serially diluted mock-treated samples and tested samples were scanned and quantified. The IC_{50} of no. 8 (72-h treatment), as determined by four repeated experiments, was 1.35 μM. (*e*) GN8 reduced PrP^{Sc} also in 22L-, Ch-, and BSE-infected cells. CR, Congo red at 10 μg/ml; PK, proteinase K digestion. (*f*) Kaplan–Meier's survival curves of FK-infected mice administered GN8 by intraventricular infusion. The control group (n = 6) was killed at 123.8 ± 7.4 days (black line). Average survival time of GN8-treated mice was 132.3 ± 9.2 days (42–70 d.p.i. group, n = 7, red line) and 141.5 ± 18.8 days (70–98 d.p.i. group, n = 6, green line). (*g*) Kaplan–Meier's survival curves of FK-infected mice administered GN8 subcutaneously. The control group (n = 9) was killed at 133.0 ± 4.9 days (black line). Average survival time of GN8-treated mice was 148.6 ± 10.3 days (67–95 d.p.i. group, n = 8, red line) and 151.4 ± 15.3 days (67–123 d.p.i. group, n = 10, green line).

production in the GT+FK at 10 μM (Fig. 1*c*). The other compounds either had little effect even at a higher dose (IC_{50} > 100 μM) or were highly toxic to the cells at 1 μM. The effect of the compound (now designated GN8) was dose-dependent (Fig. 1*d*), and by repeating the experiment we established that the effective concentration for 50% reduction of PrP^{Sc} (IC_{50}) over 72 h was ≈1.35 μM. The normal PrP^C expression in uninfected cells was unaffected. A similar effect was confirmed by using other scrapie-infected GT cells (GT+22L and GT+Ch) (20), and also by using GT+BSE cells stably infected with mouse-adapted bovine spongiform encephalopathy (BSE) (Fig. 1*e*). This confirms that the action of GN8 is not strain-specific. To see the effect of GN8 *in vivo*, mice inoculated with 20 μl of 10% FK-1 mouse brain homogenate were given the compound at a dose of 250 μg/kg per day by intraventricular infusion using osmotic pumps (Alzet Durect, Cupertino, CA) during 42–70 days post-inoculation (d.p.i.) or 70–98 d.p.i. Although the vehicle-only control (5% glucose/saline) showed that the average survival time was 123.8 ± 7.4 (n = 6), as expected, the GN8-treated mice showed slightly but significantly prolonged survival even after the appearance of clinical signs [132.3 ± 9.2 days (n = 7) in the 42–70 d.p.i. group and 141.5 ± 18.8 days (n = 6) in the 70–98 d.p.i. group; $P < 0.05$], as shown in Fig. 1*f*. The effect on the survival of infected mice is limited here because of the transient administration of GN8.

The mice administrated subcutaneously with GN8 at a dose of 8.9 mg/kg per day using infusion pumps survived longer than control mice. Whereas the control [5% glucose/saline (63–120 d.p.i. group)] showed that the average survival time was 133.0 ± 4.9 days (n = 9), the GN8-treated mice showed slightly but significantly prolonged survival [148.6 ± 10.3 days (n = 8) in the 67–95 d.p.i. group and 151.4 ± 15.3 days (n = 10) in the 67–123 d.p.i. group; $P < 0.01$], as shown in Fig. 1*g*. Pharmacological analysis using labeled GN8 is currently going on. On the other hand, pentosan polysulfate was not effective at all on the survival time when given peripherally (data not shown). Thus, GN8 could be a potential lead compound for prion diseases.

Binding of GN8 to PrP^C was confirmed by the surface plasmon resonance (21), and its dissociation constant was estimated to be 3.9 ± 0.2 × 10^{-6} M from the Scatchard plot (Fig. 2*a*; see also SI Fig. 5 and *SI Methods*). To identify the putative sites for interaction of GN8 with PrP, we analyzed the chemical shift perturbation of ^1H-^{15}N heteronuclear single quantum coherence NMR spectra (22) of a uniformly ^{15}N-labeled PrP. A comparison of the spectra revealed that three cross peaks (corresponding to V189, K194, and E196) shifted significantly upon the addition of GN8 (Fig. 2*b*), apparently in a fast-exchange mode. The GN8 concentration did not appear to significantly affect line broadening. Most of the perturbed residues were located in the S2-A loop, the B-helix, or the B-C loop regions, indicating the specific binding between GN8 and PrP^C (Fig. 2*c*). Fig. 2*d* shows the markedly perturbed residues mapped onto a three-dimensional PrP model.

To investigate whether GN8 indeed stabilizes the PrP^C conformation, we measured the thermal stability using CD. The thermal unfolding curves of recombinant mouse PrP, monitored by the molar ellipticity at 222 nm, representing the helical content of PrP and the overall unfolding behavior with (red) or without (blue) GN8, were compared quantitatively (Fig. 2*e* and

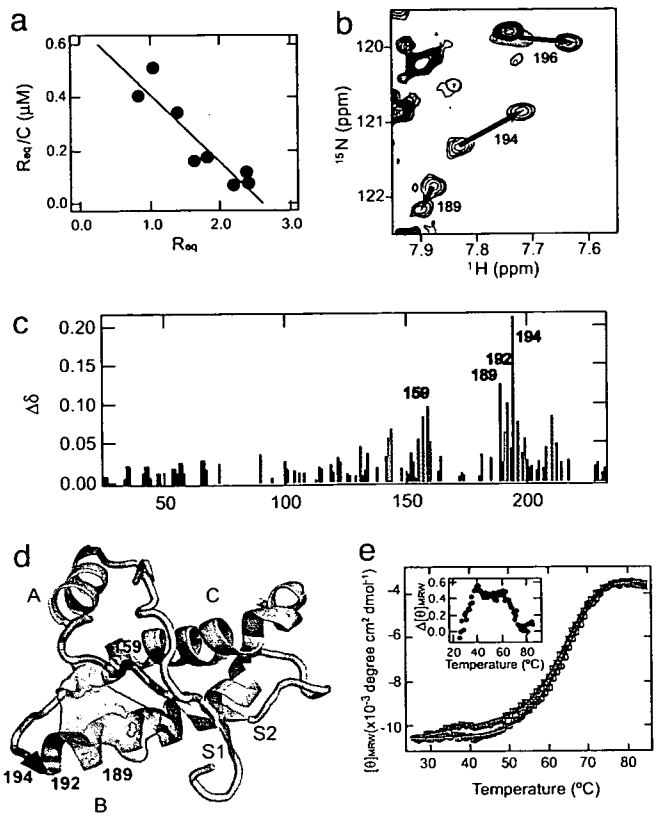

Fig. 2. Interaction of an anti-prion compound, GN8, and a recombinant mouse PrP^C. (*a*) Scatchard plot (Req vs. Req/C, where Req and C are the equilibrium response of SPR and the concentration of GN8, respectively) of the specific binding of GN8 with the PrP obtained by a surface plasmon resonance sensorgram. From the slope of the line, K_d was estimated to be 3.9 μM. (Details are shown in SI Fig. 5 and *SI Methods*.) (*b*) An overlay of the ^1H-^{15}N heteronuclear single quantum coherence NMR spectra of PrP in the absence and presence of GN8. Blue contours show the spectrum of PrP^C without GN8, and red contours show the spectrum in the presence of 1.0 mM GN8 at pH 4.5. (*c*) Plot of the weighted averages of the ^1H and ^{15}N chemical shift changes, calculated by using the function $\Delta\delta = [(\Delta\delta_{1H})^2 + 0.17(\Delta\delta_{15N})^2]^{1/2}$ against the residue number. The absence of bars in the plot indicates unassigned residues, proline residues, or unmeasured shifts due to resonance overlaps. Perturbed residues with Δδ values of >0.9 ppm are shown in red, and those with 0.9 > Δδ > 0.5 ppm are in orange. (*d*) Mapping of the perturbed residues on the structure of mPrP(121–231) (PDB entry 1AG2). The perturbed residues with Δδ values of >0.9 ppm are shown in red, and those with 0.9 > Δδ > 0.5 ppm are in orange. Binding pocket is overlaid in green. S1, A, S2, B, and C indicate S1 strand, helix A, S2 strand, helix B, and helix C, respectively. The image was created by using PyMol. (*e*) Thermal unfolding profiles of recombinant mouse PrP (amino acids 23–231, 5 μM) without (blue) or with (red) GN8 (10 μM). CD intensities of PrP in the presence of GN8 were normalized to those of PrP without GN8, and fitted curves (see *SI Methods*) are also shown. Binding with GN8 stabilizes the conformation of PrP^C. (*Inset*) The difference in extinction coefficients at 222 nm of PrP without GN8 and those in the presence of GN8, as a function of temperature.

SI Methods). Parameter sets obtained by a nonlinear fit, i.e., melting temperature (T_m) and enthalpy change (ΔH), without GN8 were 65.3 ± 0.4°C and 35.0 ± 1.9 kcal/mol, respectively, whereas those with GN8 were 67.7 ± 0.6°C and 41.8 ± 2.2 kcal/mol, respectively. This indicates that the binding of GN8 stabilizes the PrP^C conformation significantly. Intriguingly, the accumulation of the intermediate was demonstrated by an early increase in ellipticity at ≈40°C before the global unfolding as shown in Fig. 2*e Inset*. However, this is strongly suppressed in the presence of GN8. Thus, GN8 suppressed the production of both PrP^{Sc} (Fig. 1 *c–e*) and PrP^U (thermally unfolded state) (Fig. 2*e*) by reducing the intermediate population (14).

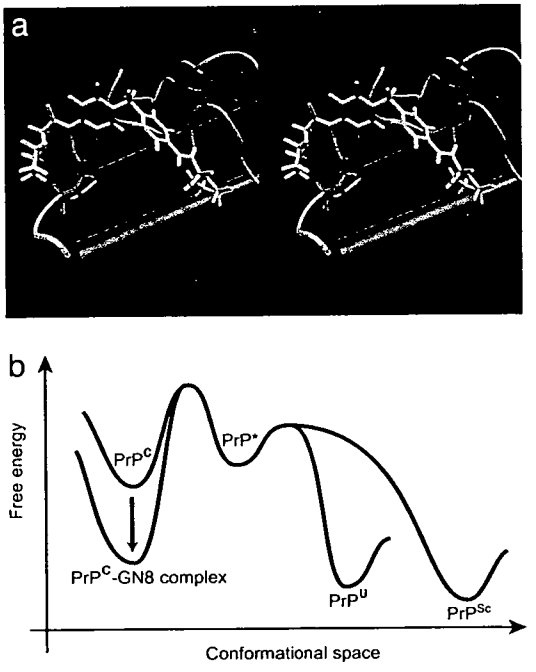

Fig. 3. Inhibitory mechanism of GN8 for pathogenic conversion. (*a*) Stereoview of the optimized complex structure of the GN8 and mouse PrP^C, with putative hydrogen bonds, calculated by using ICM version 3.0. Presumed hydrogen bonds between GN8 (green) and E196 (red) and between GN8 (green) and N159 (blue) are shown in orange (dotted lines). The images were created with VMD (52). (*b*) Illustration of the Gibbs free energy as a function of the conformational space to explain the inhibitory mechanism of a chemical chaperone, GN8. GN8 stabilizes the PrP^C conformation and reduces the population of PrP*, PrP^{Sc}, and PrP^U. PrP* may not interact with GN8, because the specific conformation around the binding sites would be lost (14). Thus, the free energy level of PrP*, PrP^U, and PrP^{Sc} would not change much in the presence of GN8.

Discussion

The structure of the PrP^C–GN8 complex was further analyzed by computer simulation using the refined energy minimization procedure with flexible receptor side chain. GN8 (Fig. 3*a*) connected distant residues, N159 (A-S2 loop) and E196 (B-C loop), by hydrogen bonds. The regions with the significant chemical shift changes described above (Fig. 2*d*) were in good agreement with the binding regions of GN8 in the simulated structure of the prion–GN8 complex (Fig. 3*a*). Intriguingly, K194 at the C terminus of the helix B and E196 in the B-C loop undergo slow exchange dynamics (16) (SI Fig. 4*b*). Indeed, the mutation E196K causes a rapidly progressive dementia and ataxia (23) and could be expected to greatly reduce the protein stability because of the elimination of salt bridges between E196, R156, and K194 (23).

Intercalation of these two binding regions (A-S2 loop and B-C loop) may be essential to stabilize the PrP^C conformation. For example, two representative binding sites, N159 and E196, are close together (distance between C_α atoms ≈ 15.4 Å) in PrP^C structure (12), but in the hypothetical PrP^{Sc} structure (24) they are considerably more distant (distance between C_α atoms ≈ 45.2 Å). Because GN8 connects distant regions (N159 and E196) in the PrP sequence (36 aa) by hydrogen bonds, large conformational shift may be significantly prohibited, and thus intermediate (PrP*) and further PrP^{Sc} or PrP^U formation may be also blocked.

Matsuda *et al.* (25) reported about the chemical chaperone therapy for GM1-gangliosidosis, but there has been no direct evidence for such a mechanism working on the anti-prion com-

pounds. Experimental evidences presented here fully support the concept that GN8 acts as a chemical chaperone to stabilize the normal prion protein (PrP) conformation. As illustrated in Fig. 3*b*, free energy of PrP^C–GN8 complex is significantly less than that of PrP^C, so the populations of the transition state, PrP*, PrP^U, and PrP^{Sc} may be reduced accordingly.

Over the past 10 years there have been various efforts to find out small compounds to reduce PrP^{Sc} population. These include porphyrins (26, 27), Congo red and its derivatives (28–30), acridine and phenothiazine derivatives (17, 31, 32), heparan sulfate (33), aminoglycan, and polyamines (34, 35). Simultaneously, various technological developments have been reported including structure-based drug design (36) followed by the structure–activity relationship study (37), small interfering RNA (38), library screening (18), high-throughput screening (39), chimeric ligand approach (40), and so on. Although strategies for drug discovery used in these studies have a broad spectrum from empirical to rational preponderance, there has been no report on the residue-specific evidences for the binding regions of anti-prion compounds. For instance, the effect of BF-168 depends on the strains (41), suggesting that BF-168 may not interact with PrP^C but with PrP^{Sc} in a strain-dependent manner, but this is still indirect evidence.

The structure of GN8 somewhat resembles a number of other small PrP^{Sc} inhibitors, such as the Congo red, which is able to interact with the N-terminal domain of PrP^C (42). However, we could not find out any evidence for the interaction between GN8 and the N-terminal domain. The inhibitory mechanism of GN8 and that of Congo red seem to be quite different because of the following reasons: (*i*) Congo red has two sulfonates on the edge of the molecule, but GN8 does not have negative charge. Thus, GN8 may not strongly interact with His+ at the octapeptide repeats of the N-terminal domain. (*ii*) Although Congo red can cause aggregation of recombinant PrP^C (42), GN8 never causes aggregation even at a relatively high concentration (≈0.03 mM) in NMR tube. (*iii*) Chemical shift changes caused by binding with GN8 are not significant at the N-terminal half region as shown in Fig. 2*c*. (*iv*) SPR affinity profile between GN8 and the C-terminal half of PrP^C(120–230) and that between GN8 and the full-length PrP^C(23–231) were quite similar, and the calculated dissociation constants were also close (≈5 μM), supporting our conclusion that the major binding regions of GN8 locate at the C-terminal domain. On the other hand, the interaction sites of GN8 with the GPI-anchored PrP^C on the cell surface could be different from those with the free PrP^C. However, a carboxymethyl moiety on the SPR sensor chip has a negative charge like a phosphate moiety on the cell membrane. Because electrostatic environments surrounding GN8 and prion on these surfaces are similar, GN8 may also interact with the C-terminal domain of the GPI-anchored PrP^C.

We found here the effective anti-prion compound GN8, which specifically binds with the hot spots undergoing the slow fluctuation on the time scale of microseconds to milliseconds and exclusively interferes with the pathogenic conversion. According to the dynamics-based drug discovery strategy, we found >20 compounds with any anti-prion activity, and the hit rate is ≈10% at present (data not shown). However, no compound has been more effective than GN8. For instance, we found a compound, GN4 (see SI Table 1), whose structure is quite similar to GN8, but the computer simulation suggested that the binding sites are R156 and N159, which are quite close (2 aa). Thus, GN4 is expected to have less inhibitory effect on the global fluctuation of PrP^C, and indeed IC_{50} of GN4 was >100 μM (data not shown).

To potentially become of any use clinically, GN8 will need to clear many pharmacological hurdles; however, our basic principle presented here constitutes a promising strategy with which to approach the discovery of therapeutic compounds for TSE. Additionally, application of the dynamics-based drug discovery approach, based on the experimentally identified hot spot (43), will make the mass screening of chemical compounds more efficient, especially for diseases related to protein misfolding (44).

Materials and Methods

Virtual Ligand Screening. We performed *in silico* screening of ligands on 320,000 compounds in the Available Chemicals Directory (MDL Information Systems, San Leandro, CA) for specific binding to mouse PrP^C (12). Residues with the exchange time constant, τ_{ex}, between two sites of >10 ms are displayed in SI Fig. 4*a* (16). The software used was ICM version 3.0 (Molsoft, La Jolla, CA). The program, by global optimization of the entire flexible ligand in the receptor (mouse PrP^C) field (45), came up with 624 candidates potentially capable of binding to the pocket with a binding score better (i.e., less) than −32, which roughly corresponds to binding energy (kcal/mol). Then, a more refined energy-minimization procedure using a flexible receptor side chain was conducted and further selected the compounds that formed hydrogen bonds with at least one of the 14 amino acids.

Chemical Compounds. Chemical compounds selected from our virtual ligand screening simulation were purchased from Aldrich Chemical Company (Milwaukee, WI), G & J Research Chemicals (Devon, U.K.), Wako Pure Chemical (Osaka, Japan), Interchim (Montlucon, France), Labotest (Niederschoena, Germany), Florida Center for Heterocyclic Compounds (Gainesville, FL), ChemBridge (San Diego, CA), Maybridge Chemical Company (Cornwall, U.K.), TimTec (Newark, NJ), Ambinter (Paris, France), Oak Samples (Kier, U.K.), Scientific Exchange (Center Ossipee, NH), ChemStar (Moscow, Russia), ChemDiv (San Diego, CA), and AsInEx (Moscow, Russia), or kindly provided by the Drug Synthesis and Chemistry Branch, Developmental Therapeutic Program, Division of Cancer Treatments and Diagnosis, National Cancer Institute. Detailed information on the sources for all of the compounds is shown in SI Table 1. The compounds were dissolved with DMSO for the *in vitro* screening and with distilled water for the spectral measurements. GN8 hydrochloride salt was prepared for *in vivo* test as follows: GN8 was first dissolved with dioxane and added to 3 N HCl in dioxane. The solvent was evaporated *in vacuo*, and the residue was recrystallized from acetone to give the hydrochloride salt of GN8. GN8 hydrochloride salt (2-pyrrolidin-1-yl-*N*-[4-[4-(2-pyrrolidin-1-yl-acetylamino)-benzyl]-phenyl]-acetamide dihydrochloride); white solid; anal. calcd. for $C_{25}H_{34}Cl_2N_4O_2$: C, 60.85; H, 6.94; Cl, 14.37; N, 11.35; O, 6.48. %Found: C, 60.83; H, 6.95; N, 11.35.

Recombinant Mouse PrP. The DNA of mouse PrP(23–231) was amplified by PCR and cloned into the expression vector pET101/D-TOPO (Invitrogen, Carlsbad, CA). As shown in *SI Methods*, the ^{15}N-labeled recombinant PrP for NMR measurements was expressed in *Escherichia coli* strain BL21 Star (DE3) (Invitrogen), grown in ^{15}N-labeled minimum medium Spectra9 (Spectra Gases, Branchburg, NJ), and purified by a Ni-chelating affinity chromatography method (46). Oxidization and refolding of the purified protein (47) were performed in buffer containing 4 M urea at pH 8. A recombinant PrP sample for the surface plasmon resonance sensorgram experiment was obtained by a similar procedure using a non-isotope-labeled LB medium instead of the Spectra9.

Cell Culture and Antibodies. The immortalized mouse neuronal cell line GT1-7 was cultured as described (20). GT1-7 cells stably infected with Fukuoka-1, 22L, or Chandler/RML (designated GT+FK, GT+22L, or GT+Ch, respectively) were maintained for more than a year in our laboratory. GT+BSE cells were infected *ex vivo* in our laboratory with mouse-adapted BSE agent (a kind gift from T. Yokoyama, National Institute of Animal Health, Tsukuba, Japan). Stock solutions of compounds were prepared fresh in 100%

DMSO at 100 mM and stored at 4°C. Before use, compounds were diluted with medium as indicated. Control cells were treated with medium containing solvent alone (0.1%). Approximately 2×10^5 cells were plated in each well of a six-well plate, and drug treatment was started 15 h later. After 72 h of incubation, cells were lysed in 150 μl of 1× Triton X-100/DOC lysis buffer (48), and samples normalized to 2 mg of protein per milliliter. Western blotting for PrP^{Sc} was done as described previously (48). Anti-mouse PrP antisera (SS28) (49) and SAF32 antibody (SPI-BIO, Montigny le Bretonneux, France) were used for PrP^{Sc} and PrP^{C}, respectively, as the primary antibody. The signals were visualized by ECL-plus (Amersham, Buckinghamshire, U.K.) and scanned by using Fluor-Chem (Alpha Innotech, San Leandro, CA).

NMR Measurements and Data Analysis. For NMR measurements, 0.6 mg/ml ^{15}N-uniformly labeled mouse PrP(23–231) was prepared in 30 mM acetate-d_3 buffer (pH 4.5) containing 1 mM NaN_3, 4.5 μM 4-(2-aminoethyl)-benzenesulfonyl fluoride hydrochloride, 20 μM EDTA, 0.4 μM Bestatin, 0.06 μM pepstatin, 0.06 μM E-64, and 1 nM sodium 2,2-dimethyl-2-silapentane-5-sulfonate dissolved in 90% H_2O/10% D_2O. NMR spectra were recorded at 20.0°C on an Avance600 spectrometer (Bruker, Rheinstetten, Germany) at Gifu University. The spectrometer operates at ^1H frequency of 600.13 MHz and ^{15}N frequency of 60.81 MHz. A 5-mm ^1H inverse detection probe with triple-axis gradient coils was used for all measurements. ^1H-^{15}N heteronuclear single quantum coherence spectra were acquired with 2,048 complex points covering 9,600 Hz for ^1H and 256 complex points covering 1,200 Hz for ^{15}N. NMR data were processed by using the XWIN-NMR software package (Bruker) and Sparky (50). Resonance frequencies in these spectra were identified by using the chemical shift lists on mouse PrP(23–231) and PrP (121–231) (51). For the chemical shift perturbation experiments, aliquots of 2.5 μl of 0, 10, or 100 mM GN8 solutions in DMSO-d_6 were added to 0.6 mg/ml ^{15}N PrP(23–231) in a 5-mm-diameter Shigemi microtube; the final concentration of GN8 is 0, 1, and 10 mM, respectively. The backbone ^1H and ^{15}N chemical shifts for the GN8-bound protein were assigned by tracing the corresponding peaks in ^1H-^{15}N heteronuclear single quantum coherence spectra measured at various concentrations of GN8.

Preparation of GN8 for Injection and *in Vivo* Test. The GN8 hydrochloride salt was dissolved in saline with 5% glucose and sterilized by passing through a 0.2-μm filter. The concentration of the stock solution was adjusted to 10 mg/ml and kept at 4°C until use. Ten percent FK-infected brain homogenate was inoculated into right temporal lobes of 4-week-old male mice (ddY), followed by intraventricular infusion of GN8 using an osmotic pump. Six or 10 weeks after inoculation, an osmotic pump was inserted subcutaneously and the infusion cannula was implanted into the right ventricle. The pump was filled with GN8 (1.4 mg/ml) or saline with 5% glucose. In a parallel experiment, pentosan polysulfate (Bene, Munich, Germany) was administered at 200 μg/kg per day by intraventricular or i.p. infusion. All mice were carefully examined daily for neurological signs, and the incubation period was monitored. Survival data were statistically evaluated according to Kaplan–Meier's method using StatMateIII (ATMS, Tokyo, Japan).

In case of subcutaneous infusion of GN8, the concentration of the stock solution was adjusted to 50 mg/ml. One percent FK-infected brain homogenate was inoculated in the same way, and an osmotic pump including GN8 was inserted subcutaneously at 9 weeks after inoculation.

Some compounds were kindly provided by the Drug Synthesis and Chemistry Branch, Developmental Therapeutic Program, Division of Cancer Treatments and Diagnosis, National Cancer Institute. We thank Ms. Sakiko Morishita and Mr. Yuki Matsui for technical help. K. Kuwata was supported in part by Grants-in-Aid for Scientific Research from the Ministry of Education, Culture, Sports, Science and Technology of Japan and grants from the Ministry of Health, Labour, and Welfare. This study was supported by the Program for Promotion of Fundamental Studies in Health Sciences of the National Institute of Biomedical Innovation.

1. Prusiner SB (1982) *Science* 216:136–144.
2. Prusiner SB (1991) *Crit Rev Biochem Mol Biol* 26:397–438.
3. Prusiner SB (1998) *Proc Natl Acad Sci USA* 95:13363–13383.
4. Bueler H, Aguzzi A, Sailer A, Greiner RA, Autenried P, Aguet M, Weissmann C (1993) *Cell* 73:1339–1347.
5. Sailer A, Bueler H, Fischer M, Aguzzi A, Weissmann C (1994) *Cell* 77:967–968.
6. Cohen FE, Pan KM, Huang Z, Baldwin M, Fletterick RJ, Prusiner SB (1994) *Science* 264:530–531.
7. Peretz D, Williamson RA, Legname G, Matsunaga Y, Vergara J, Burton DR, DeArmond SJ, Prusiner SB, Scott MR (2002) *Neuron* 34:921–932.
8. Zhang CC, Steele AD, Lindquist S, Lodish HF (2006) *Proc Natl Acad Sci USA* 103:2184–2189.
9. Donne DG, Viles JH, Groth D, Mehlhorn I, James TL, Cohen FE, Prusiner SB, Wright PE, Dyson HJ (1997) *Proc Natl Acad Sci USA* 94:13452–13457.
10. James TL, Liu H, Ulyanov NB, Farr-Jones S, Zhang H, Donne DG, Kaneko K, Groth D, Mehlhorn I, Prusiner SB, Cohen FE (1997) *Proc Natl Acad Sci USA* 94:10086–10091.
11. Gossert AD, Bonjour S, Lysek DA, Fiorito F, Wuthrich K (2005) *Proc Natl Acad Sci USA* 102:646–650.
12. Riek R, Hornemann S, Wider G, Billeter M, Glockshuber R, Wuthrich K (1996) *Nature* 382:180–182.
13. Lysek DA, Schorn C, Nivon LG, Esteve-Moya V, Christen B, Calzolai L, von Schroetter C, Fiorito F, Herrmann T, Guntert P, Wuthrich K (2005) *Proc Natl Acad Sci USA* 102:640–645.
14. Kuwata K, Li H, Yamada H, Legname G, Prusiner SB, Akasaka K, James TL (2002) *Biochemistry* 41:12277–12283.
15. Korzhnev DM, Salvatella X, Vendruscolo M, Di Nardo AA, Davidson AR, Dobson CM, Kay LE (2004) *Nature* 430:586–590.
16. Kuwata K, Kamatari YO, Akasaka K, James TL (2004) *Biochemistry* 43:4439–4446.
17. Doh-Ura K, Iwaki T, Caughey B (2000) *J Virol* 74:4894–4897.
18. Kocisko DA, Baron GS, Rubenstein R, Chen J, Kuizon S, Caughey B (2003) *J Virol* 77:10288–10294.
19. Lipinski CA, Lombardo F, Dominy BW, Feeney PJ (2001) *Adv Drug Deliv Rev* 46:3–26.
20. Milhavet O, McMahon HE, Rachidi W, Nishida N, Katamine S, Mange A, Arlotto M, Casanova D, Riondel J, Favier A, Lehmann S (2000) *Proc Natl Acad Sci USA* 97:13937–13942.
21. Touil F, Pratt S, Mutter R, Chen B (2006) *J Pharm Biomed Anal* 40:822–832.
22. Zuiderweg ER (2002) *Biochemistry* 41:1–7.
23. Peoc'h K, Manivet P, Beaudry P, Attane F, Besson G, Hannequin D, Delasnerie-Laupretre N, Laplanche JL (2000) *Hum Mutat* 15:482.
24. Govaerts C, Wille H, Prusiner SB, Cohen FE (2004) *Proc Natl Acad Sci USA* 101:8342–8347.
25. Matsuda J, Suzuki O, Oshima A, Yamamoto Y, Noguchi A, Takimoto K, Itoh M, Matsuzaki Y, Yasuda Y, Ogawa S, *et al.* (2003) *Proc Natl Acad Sci USA* 100:15912–15917.
26. Caughey WS, Raymond LD, Horiuchi M, Caughey B (1998) *Proc Natl Acad Sci USA* 95:12117–12122.
27. Priola SA, Raines A, Caughey WS (2000) *Science* 287:1503–1506.
28. Caspi S, Halimi M, Yanai A, Sasson SB, Taraboulos A, Gabizon R (1998) *J Biol Chem* 273:3484–3489.
29. Milhavet O, Mange A, Casanova D, Lehmann S (2000) *J Neurochem* 74:222–230.
30. Sellarajah S, Lekishvili T, Bowring C, Thompsett AR, Rudyk H, Birkett CR, Brown DR, Gilbert IH (2004) *J Med Chem* 47:5515–5534.
31. Korth C, May BC, Cohen FE, Prusiner SB (2001) *Proc Natl Acad Sci USA* 98:9836–9841.
32. May BC, Fafarman AT, Hong SB, Rogers M, Deady LW, Prusiner SB, Cohen FE (2003) *Proc Natl Acad Sci USA* 100:3416–3421.
33. Adjou KT, Simoneau S, Sales N, Lamoury F, Dormont D, Papy-Garcia D, Barritault D, Deslys JP, Lasmezas CI (2003) *J Gen Virol* 84:2595–2603.
34. Perez M, Wandosell F, Colaco C, Avila J (1998) *Biochem J* 335:369–374.
35. Supattapone S, Nguyen HO, Cohen FE, Prusiner SB, Scott MR (1999) *Proc Natl Acad Sci USA* 96:14529–14534.
36. Perrier V, Wallace AC, Kaneko K, Safar J, Prusiner SB, Cohen FE (2000) *Proc Natl Acad Sci USA* 97:6073–6078.
37. May BC, Zorn JA, Witkop J, Sherrill J, Wallace AC, Legname G, Prusiner SB, Cohen FE (2007) *J Med Chem* 50:65–73.
38. Daude N, Marella M, Chabry J (2003) *J Cell Sci* 116:2775–2779.

39. Bertsch U, Winklhofer KF, Hirschberger T, Bieschke J, Weber P, Hartl FU, Tavan P, Tatzelt J, Kretzschmar HA, Giese A (2005) *J Virol* 79: 7785–7791.
40. Dollinger S, Lober S, Klingenstein R, Korth C, Gmeiner P (2006) *J Med Chem* 49:6591–6595.
41. Ishikawa K, Kudo Y, Nishida N, Suemoto T, Sawada T, Iwaki T, Doh-ura K (2006) *J Neurochem* 99:198–205.
42. Caughey B, Caughey WS, Kocisko DA, Lee KS, Silveira JR, Morrey JD (2006) *Acc Chem Res* 39:646–653.
43. Clackson T, Wells JA (1995) *Science* 267:383–386.
44. Soto C, Estrada L, Castilla J (2006) *Trends Biochem Sci* 31:150–155.
45. Schapira M, Raaka BM, Samuels HH, Abagyan R (2000) *Proc Natl Acad Sci USA* 97:1008–1013.
46. Bocharova OV, Breydo L, Parfenov AS, Salnikov VV, Baskakov IV (2005) *J Mol Biol* 346:645–659.
47. Lu BY, Beck PJ, Chang JY (2001) *Eur J Biochem* 268:3767–3773.
48. Nishida N, Harris DA, Vilette D, Laude H, Frobert Y, Grassi J, Casanova D, Milhavet O, Lehmann S (2000) *J Virol* 74:320–325.
49. Nishida N, Tremblay P, Sugimoto T, Shigematsu K, Shirabe S, Petromilli C, Erpel SP, Nakaoke R, Atarashi R, Houtani T, *et al.* (1999) *Lab Invest* 79:689–697.
50. Goddard TD, Kneller DG (2001) SPARKY (Univ of California, San Francisco), Version 3.
51. Riek R (1988) PhD thesis (Swiss Federal Institute of Technology, Zürich, Switzerland).
52. Humphrey W, Dalke A, Schulten K (1996) *J Mol Graphics* 14:27–28, 33–38.

Cellular and Molecular Neurobiology, Vol. 27, No. 3, May 2007 (© 2006)
DOI: 10.1007/s10571-006-9125-x

Inhibition of Transforming Growth Factor-β Production in Brain Pericytes Contributes to Cyclosporin A-Induced Dysfunction of the Blood-Brain Barrier

Fuyuko Takata,[1,2] Shinya Dohgu,[1] Atsushi Yamauchi,[1] Noriko Sumi,[1] Shinsuke Nakagawa,[2,3] Mikihiko Naito,[4] Takashi Tsuruo,[4] Hideki Shuto,[1] and Yasufumi Kataoka[1,2,5]

Received July 24, 2006; accepted October 5, 2006; Published online: December 28, 2006

SUMMARY

1. The present study was designed to clarify whether brain pericytes and pericyte-derived transforming growth factor-β1 (TGF-β1) participate in cyclosporin A (CsA)-induced dysfunction of the blood-brain barrier (BBB).

2. The presence of brain pericytes markedly aggravated CsA-increased permeability of MBEC4 cells to sodium fluorescein and accumulation of rhodamine 123 in MBEC4 cells.

3. Exposure to CsA significantly decreased the levels of TGF-β1 mRNA in brain pericytes in pericyte co-cultures. Treatment with TGF-β1 dose-dependently inhibited CsA-induced hyperpermeability and P-glycoprotein dysfunction of MBEC4 cells in pericyte co-cultures.

4. These findings suggest that an inhibition of brain pericyte-derived TGF-β1 contributes to the occurrence of CsA-induced dysfunction of the BBB.

KEY WORDS: Cyclosporin A; brain pericytes; transforming growth factor-β; blood-brain barrier; permeability; P-glycoprotein; mouse brain endothelial cells.

INTRODUCTION

Cyclosporin A (CsA), a cyclic 11-amino acid peptide, is widely used as a potent immunosuppressant to prevent allograft rejection in solid organ transplantation and in fatal graft-versus-host disease after bone marrow transplantation; it is also used to treat various autoimmune diseases including rheumatoid arthritis

[1] Department of Pharmaceutical Care and Health Sciences, Faculty of Pharmaceutical Sciences, Fukuoka University, Jonan-ku, Fukuoka 814-0180, Japan.
[2] PharmaCo-Cell Company Ltd., Nagayo-machi, Nagasaki 851-2127, Japan.
[3] Department of Pharmacology 1, Nagasaki University School of Medicine, Sakamoto, Nagasaki 852-8501, Japan.
[4] Institute of Molecular and Cellular Biosciences, University of Tokyo, Bunkyo-ku, Tokyo 113-0032, Japan.
[5] To whom correspondence should be addressed; e-mail: ykataoka@fukuoka-u.ac.jp.

(Kahan, 1989). Despite its high efficacy, CsA has adverse effects including nephrotoxicity, cardiovascular disorders, gastrointestinal disorders and neurotoxicity. CsA-associated neurotoxicity occurs with a relatively high frequency (20–40%) in organ-transplanted patients with high blood drug levels or within the therapeutic range (The U.S. Multicenter FK506 Liver Study Group, 1994; Pirsch *et al.*, 1997; Gijtenbeek *et al.*, 1999). However, the mechanism of CsA-induced neurotoxicity remains obscure.

The entry of CsA into the brain is usually prevented by the tight junctions and P-glycoprotein (P-gp), a multi-drug efflux pump, of brain microvascular endothelial cells. But CsA-associated neurotoxicity, including tremors, seizures and encephalopathy, strongly suggests the possibility that CsA is transported across the blood-brain barrier (BBB). We previously reported that CsA produced convulsions by inhibiting γ-aminobutyric acid (GABA)ergic neural activity and the binding properties of the $GABA_A$ receptor (Shuto *et al.*, 1999). The inhibition of GABAergic neurotransmission by CsA may lead to an activation of serotonergic neural activity and, consequently, produce tremors (Shuto *et al.*, 1998). These *in vivo* findings are considered to be due to a direct action of CsA transported across the BBB rather than an indirect effect of CsA in the periphery. Indeed, we previously demonstrated that a high concentration of CsA decreased the function and expression of P-gp in brain capillary endothelial cells (Kochi *et al.*, 1999, 2000). The BBB is primarily formed from these cells, which are closely sealed by tight junctions (Pardridge, 1999). P-gp is abundantly expressed in brain endothelial cells and limits the accumulation of many hydrophobic molecules and toxic substances in the brain (Schinkel, 1999). Brain capillary endothelial cells are surrounded by two other cellular components of the BBB, astrocytes and brain pericytes. We also previously reported that the presence of astrocytes markedly aggravated CsA-induced hyperpermeability of, and P-gp dysfunction in, MBEC4 cells, through the acceleration of NO production (Dohgu *et al.*, 2004a). Brain pericytes are important for the growth and migration of endothelial cells and the integrity of microvascular capillaries (Thomas, 1999; Ramsauer *et al.*, 2002). Brain capillary endothelial cells communicate closely with brain pericytes to maintain the BBB (Hori *et al.*, 2004; Dohgu *et al.*, 2005). Transforming growth factor-β (TGF-β) is a cytokine produced by pericytes (Antonelli-Orlidge *et al.*, 1989). We previously reported that brain pericytes contribute to the up-regulation of barrier function and P-gp activity in brain endothelial cells through production of TGF-β1 (Dohgu *et al.*, 2005).

The present study was designed to clarify whether brain pericytes and pericyte-derived TGF-β participate in CsA-induced dysfunction of the BBB. We first evaluated the effect of CsA on the permeability of, and P-gp function in, mouse brain capillary endothelial (MBEC4) cells, either alone or co-cultured with human brain pericytes. Next, the effect of CsA on TGF-β1 mRNA expression in brain pericytes and the effect of TGF-β1 on CsA-decreased BBB function were examined in a co-culture system containing MBEC4 cells and brain pericytes.

MATERIALS AND METHODS

Materials

CsA was kindly supplied by Novartis Pharma (Basel, Switzerland). Sodium fluorescein (Na-F, MW 376), rhodamine 123 and human TGF-β1 were purchased from Sigma (St. Louis, MO). Culture medium and subculture reagents were obtained from Invitrogen (Carlsbad, CA). All remaining reagents of analytical grade were purchased from Wako (Osaka, Japan).

Cell Culture

MBEC4 cells, isolated from BALB/c mouse brain cortices and immortalized by SV40-transformation (Tatsuta *et al.*, 1992), were cultured in Dulbecco's modified Eagle's medium (DMEM) supplemented with 10% fetal bovine serum, 100 units/mL penicillin and 100 μg/mL streptomycin. Human brain pericytes (CS-ABI-499, Cell Systems Corporation, Kirkland, WA) were cultured in CS-C Complete Medium Kit (Cell Systems Corporation). They were grown in a humidified atmosphere of 5% CO_2/95% air at 37°C. To make an *in vitro* BBB model, brain pericytes (20,000 cells/cm^2) were first cultured in the wells of a 12-well culture plate. After 2 days, MBEC4 cells (42,000 cells/cm^2) were seeded on the inside of the collagen-coated polycarbonate membrane (1.0 cm^2, 3.0 μm pore size) of a Transwell®-Clear insert (12-well type, Costar, MA) placed in the plate containing layers of brain pericytes (pericyte co-culture). A monolayer system was also generated with MBEC4 cells alone (MBEC4 monolayer).

Cell viability was assessed using a WST-8 assay (Cell Counting Kit, DOJINDO, Kumamoto, Japan). The absorbance of a highly water-soluble formazan dye (WST-8), reduced by mitochondrial dehydrogenase, was measured in each sample at wavelengths of 450-nm (test wavelength) and 700-nm (reference wavelength).

Treatment with CsA and TGF-β1

TGF-β1 was dissolved in 4 mM HCl containing 1 mg/mL of bovine serum albumin; CsA was dissolved in ethanol. Each original solution was then diluted with serum-free medium. The final concentrations in the test media were 4 μM HCl/1 μg/mL bovine serum albumin or 0.1% ethanol. MBEC4 cells were cultured for 3 days, and the inserts were washed three times with serum-free medium. Cells were then exposed for 1–12 h to 5 μM of CsA injected into the inside of the insert (luminal side). Alternatively, TGF-β1 (0.01–1 ng/mL) was loaded on the luminal side. In parallel, cells were treated with serum-free medium containing the corresponding amount of ethanol and/or HCl and bovine serum albumin as the vehicle.

Transcellular Transport of Na-F

To initiate the transport experiments, the medium was removed and MBEC4 cells were washed three times with Krebs–Ringer buffer (118 mM NaCl, 4.7 mM

KCl, 1.3 mM $CaCl_2$, 1.2 mM $MgCl_2$, 1.0 mM NaH_2PO_4, 25 mM $NaHCO_3$, and 11 mM D-glucose, pH 7.4). Krebs–Ringer buffer (1.5 mL) was added to the outside of the insert (abluminal side). Krebs–Ringer buffer (0.5 mL) containing 100 μg/mL of Na-F was loaded on the luminal side of the insert. Samples (0.5 mL) were removed from the abluminal chamber at 10, 20, 30 and 60 min and immediately replaced with fresh Krebs–Ringer buffer. Aliquots (5 μL) of the abluminal medium were mixed with 200 μL of Krebs–Ringer buffer and the concentration of Na-F was determined using a fluorescence multiwell plate reader (Ex(λ) 485 nm; Em(λ) 530 nm) (CytoFluor Series 4000, PerSeptive Biosystems, Framingham, MA). The permeability coefficient and clearance were calculated according to the method described by Dehouck *et al.* (1992). Clearance was expressed as microliters (μL) of tracer diffusing from the luminal to abluminal chamber and was calculated from the initial concentration of tracer in the luminal chamber and final concentration in the abluminal chamber: clearance (μL) = $[C]_A \times V_A/[C]_L$ where $[C]_L$ is the initial luminal tracer concentration, $[C]_A$ is the abluminal tracer concentration and V_A is the volume of the abluminal chamber. During the 60-min period of the experiment, the clearance volume increased linearly with time. The average volume cleared was plotted against time, and the slope was estimated by linear regression analysis. The slope of clearance curves for the MBEC4 monolayer or co-culture systems was denoted by PS_{app}, where PS is the permeability–surface area product (in μL/min). The slope of the clearance curve with a control membrane was denoted by $PS_{membrane}$. The real PS value for the MBEC4 monolayer and the co-culture system (PS_{trans}) was calculated as $1/PS_{app} = 1/PS_{membrane} + 1/PS_{trans}$. The PS_{trans} values were divided by the surface area of the Transwell inserts to generate the permeability coefficient (P_{trans}, in cm/min).

Functional Activity of P-gp

The functional activity of P-gp was determined by measuring the cellular accumulation of rhodamine 123 (Sigma) according to the method of Fontaine *et al.* (1996). MBEC4 cells were washed three times with assay buffer (143 mM NaCl, 4.7 mM KCl, 1.3 mM $CaCl_2$, 1.2 mM $MgCl_2$, 1.0 mM NaH_2PO_4, 10 mM HEPES, and 11 mM D-glucose, pH 7.4), and then incubated in 0.5 mL of assay buffer containing 5 μM rhodamine 123 for 60 min. The solution was then removed and the cells were washed three times with ice-cold phosphate-buffered saline and solubilized in 1 M NaOH (0.2 mL). The solution was neutralized with 1 M HCl (0.2 mL) and the rhodamine 123 content was determined using a fluorescence multiwell plate reader (Ex(λ) 485 nm; Em(λ) 530 nm, CytoFluor Series 4000). Protein concentration was measured by the method of Bradford (Bradford, 1976).

Expression of TGF-β1 Receptor mRNA in MBEC4 Cells and Human Brain Pericytes

Reverse-transcription polymerase chain reaction (RT-PCR) was employed to determine the level of mRNA expression for TGF-β1 receptor I and II in MBEC4 cells and brain pericytes. Total RNA was extracted from cultured cells

using TRIzol™ reagent (Invitrogen, Carlsbad, CA) and 1 μg of RNA was reverse-transcribed and amplified by PCR using a SuperScript One-Step RT-PCR system (Invitrogen). Amplification was performed in a DNA thermal cycler (PC707; ASTEC, Fukuoka, Japan). The primers used and PCR conditions are summarized in Table I. Ten microliters of each PCR product was analyzed by electrophoresis on a 2% agarose (Sigma) gel with ethidium bromide staining. Gels were visualized on a UV light transilluminator and photographed using a DC290 Zoom digital camera (Kodak, Rochester, New York).

Relative Quantitation of TGF-β1 mRNA by Real-Time RT-PCR

Real-time RT-PCR was employed to determine the level of TGF-β1 gene expression in brain pericytes with CsA-treated pericyte co-culture. Total RNA was extracted from brain pericytes using TRIzol™ reagent (Invitrogen) and 2 μg RNA was reverse-transcribed using a SuperScript™ III First-Strand Synthesis System (Invitrogen) in a total volume of 20 μL, according to the manufacturer's protocol.

Real-time PCR was conducted on an Mx3000P™ Multiplex Quantitative PCR System (Stratagene, La Jolla, CA) with 2 μL of reverse-transcription product, Brilliant™ SYBR® Green QPCR Master Mix (Stratagene), primers at 150 nM and reference dye, in a total volume of 50 μL as per the manufacturer's protocol. The following PCR conditions were employed: 95°C for 10 min, followed by cycles of 95°C for 30 s, 54°C for 60 s and 72°C for 90 s. The sequences of primers were as follows: sense primer 5′-CCCTGGACACCAACTATTG-3′ and antisense primer 5′-CCGGGTTATGCTGGTTGTA-3′ for TGF-β1 (Untergasser *et al.*, 2005); sense primer 5′-GAGTCAACGGATTTGGTCGT-3′ and antisense primer 5′-TTGATTTTGGAGGGATCTCG-3′ for glyceraldehyde-3-phosphate dehydrogenase (GAPDH; GenBank Accession Number, M33197). After amplification, a melting curve was obtained by heating at 55°C and fluorescence data were collected at 0.2°C/s.

Relative quantitative analysis was performed employing Mx3000P™ Multiplex Quantitative PCR System software (Stratagene). We used the expression of GAPDH to normalize the expression data for the TGF-β1 gene. For a comparative analysis, values from vehicle treated brain pericytes were arbitrarily set as 1. Each sample was analyzed in triplicate.

Statistical Analysis

Values are expressed as means ± SEM. Statistical analysis was performed using Student's *t*-test. One-way and two-way analyses of variance (ANOVAs) followed by Tukey–Kramer's tests or Dunnett tests were applied to multiple comparisons. The differences between means were considered to be significant when P values were less than 0.05.

RESULTS

To obtain molecular evidence for the expression of TGF-β receptor I and II in MBEC4 cells and human brain pericytes, RT-PCR was carried out with a primer

Table I. Nucleotide Sequences of Probes Used in RT-PCR Assays and Amplification Conditions

Gene	Source (reference)	Sequence	Product (bp)	Amplification conditions
TGF-β R I	Mouse (Machida *et al.*, 2000)	Sense 5′-ATCCATCACTAGATCGCCCT-3′ Antisense 5′-CGATGGATCAGAAGGTACAAGA-3′	824	94°C for 30 s, 57°C for 30 s, 72°C for 30 s
	Human (GenBank Accession Number, L11695)	Sense 5′-GATGGGCTCTGCTTTGTCTC-3′ Antisense 5′-CAAGGCCAGGTGATGACTTT-3′	214	94°C for 30 s, 54°C for 30 s, 72°C for 30 s
TGF-β R II	Mouse (Machida *et al.*, 2000)	Sense 5′-CGTGTGGAGGAAGAACAACA-3′ Antisense 5′-TCTCAAACTGCTCTGAGGTG-3′	560	94°C for 30 s, 57°C for 30 s, 72°C for 30 s
	Human (GenBank Accession Number, E10743)	Sense 5′-TTTTCCACCTGTGACAACCA-3′ Antisense 5′-GGAGAAGCAGCATCTTCCAG-3′	185	94°C for 30 s, 54°C for 30 s, 72°C for 30 s

pair specific to each type of TGF-β receptor, from either mouse (for use on MBEC4 cells) or human (for use on human brain pericytes). As shown in Fig. 1A, RT-PCR with mRNA obtained from either MBEC4 cells or brain pericytes yielded a single product. The size of these products was as expected from the primer positions.

When MBEC4 cells were co-cultured with pericytes, the Na-F permeability of MBEC4 cells was increased from 3.26 ± 0.13 × 10^{-4} cm/min in monolayers to 3.86 ± 0.23 × 10^{-4} cm/min (Fig. 1C). The presence of pericytes decreased rhodamine 123 accumulation in MBEC4 cells from 0.51 ± 0.12 nmol/mg protein in monolayers to 0.43 ± 0.10 nmol/mg protein (Fig. 1D). A 12 h-exposure to CsA at 5 or 10 μM showed no effect on cell viability as determined by mitochondrial dehydrogenase activities (WST-8 assay) of MBEC4 cells in MBEC4 monolayers

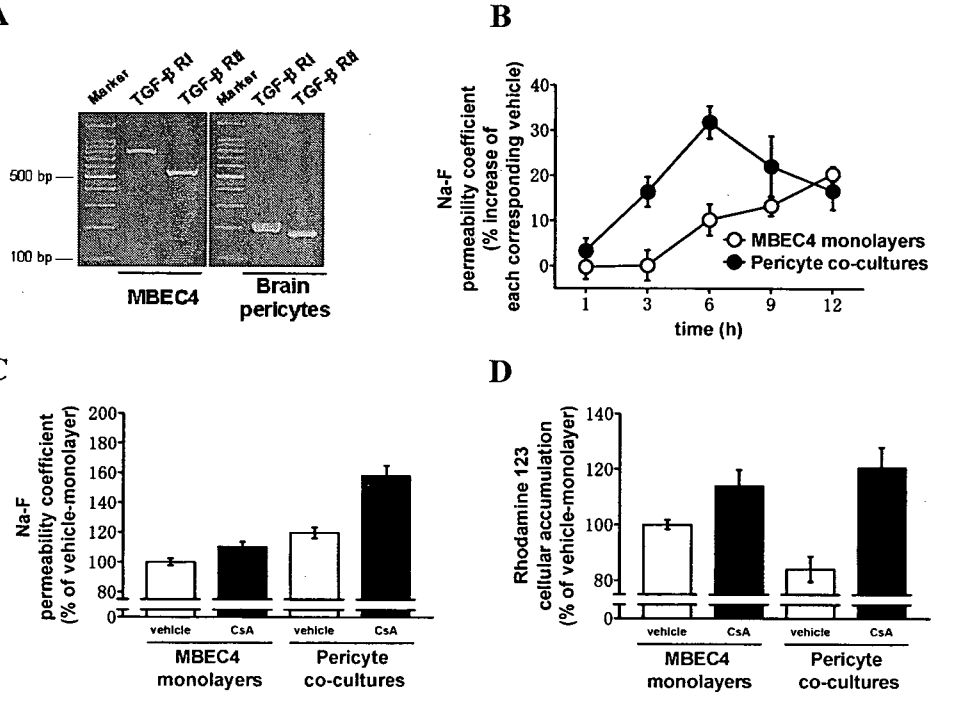

Fig. 1. (A) Expression of TGF-β receptor I and II mRNA in MBEC4 cells and human brain pericytes by RT-PCR analysis. (B) Time-course of the effect of CsA (5 μM) on the Na-F permeability of MBEC4 cells in MBEC4 monolayers and pericyte co-cultures. Transport experiments were performed after 1, 3, 6, 9 and 12 h of exposure to CsA. Results are expressed as % increase of each corresponding vehicle treatment (MBEC4 monolayers; 2.78 ± 0.10 × 10^{-4} to 3.47 ± 0.14 × 10^{-4} cm/min, pericyte co-cultures; 3.24 ± 0.10 × 10^{-4} to 4.47 ± 0.20 × 10^{-4} cm/min). Values are the means ± SEM (n = 7–16). (C) Effect of treatment with CsA (5 μM) for 6 h on the Na-F permeability of MBEC4 cells in MBEC4 monolayers and pericyte co-cultures. Results are expressed as % of vehicle-treated MBEC4 monolayers (% of vehicle-monolayer (3.26 ± 0.13 × 10^{-4} cm/min)). Values are the means ± SEM (n = 7). (D) Effect of treatment with CsA (5 μM) for 6 h on the rhodamine 123 accumulation of MBEC4 cells in MBEC4 monolayers and pericyte co-cultures. Results are expressed as % of vehicle-treated MBEC4 monolayers (% of vehicle-monolayer (0.51 ± 0.12 nmol/mg protein)). Values are the means ± SEM (n = 8).

(100.0 ± 1.8 and 103.1 ± 7.8% of vehicle, respectively, $n = 4$ inserts) and pericyte co-cultures (99.2 ± 2.5 and 106.8 ± 2.3% of vehicle, respectively, $n = 4$ inserts). Figure 1C and D shows the effect of CsA (5 μM) on the permeability of MBEC4 cells to Na-F and the accumulation of rhodamine 123 in MBEC4 cells, respectively, in both MBEC4 monolayers and pericyte co-cultures. The Na-F permeability of MBEC4 cells was time-dependently increased during a period of 1–6 h after the addition of CsA (5 μM), reaching a peak at 6 h (Fig. 1B). A significant difference in CsA-induced hyperpermeability was observed between MBEC4 monolayers and pericyte co-cultures, with the effect being most apparent after a 6 hexposure [$F(1, 24) = 10.51$, $P < 0.01$] (Fig. 1C). At the peak time, CsA increased the Na-F pearmeability of MBEC4 cells by 10.3 ± 3.4 and 31.9 ± 3.6% of each corresponding vehicle treatment in MBEC4 monolayers and pericyte co-cultures, respectively (Fig. 1C). Following exposure of cells to CsA for 9–12 h, permeability of the MBEC4 monolayers was gradually increased. However, the effect of CsA on pericyte co-cultures permeability became more moderate, reducing to the same level seen in MBEC4 monolayers (Fig. 1B). To clarify the role of brain pericytes in CsA-induced dysfunction of BBB, a 6 h-exposure of cells to CsA (5 μM) was employed in the following experiment. The accumulation of rhodamine 123 in MBEC4 cells was increased by 13.9 ± 5.9 and 43.4 ± 8.5% of each corresponding vehicle treatment in MBEC4 monolayers and pericyte co-cultures, respectively, after a 6 h-exposure to CsA (Fig. 1D). A significant difference in CsA-induced decrease in P-gp activity was observed between MBEC4 monolayers and pericyte co-cultures [$F(1, 28) = 4.65$, $P < 0.05$]. CsA-induced inhibition of P-gp function was more potent in pericyte co-cultures than in MBEC4 monolayers.

When pericyte co-cultures were treated with CsA (5 μM) for 6 h, the levels of TGF-β1 mRNA in brain pericytes were significantly decreased to 81.0 ± 7.3% of vehicle (Fig. 2A) [$F(2, 13) = 5.05$, $P < 0.05$]; however, a 12 h exposure to CsA failed to decrease levels of TGF-β1 mRNA in brain pericytes (103.8 ± 10.8% of vehicle). In pericyte co-cultures, TGF-β1 (0.01–1 ng/mL) dose-dependently inhibited the elevation of Na-F permeability (Fig. 2B), and rhodamine 123 accumulation (Fig. 2C), in MBEC4 cells, induced by CsA (132.9 ± 11.4 to 105.4 ± 2.5% and 140.3 ± 9.9 to 98.6 ± 6.4% of vehicle, respectively).

DISCUSSION

In the present study, CsA (5 μM) time-dependently increased the Na-F permeability of MBEC4 cells in pericyte co-cultures, this effect reaching a peak at 6 h after the addition of CsA (Fig. 1B and C). A 6 h-exposure to CsA also decreased P-gp function in MBEC4 cells in pericyte co-cultures, this effect being more apparent than that in MBEC4 monolayers (Fig. 1D). These findings suggest that CsA-induced hyperpermeability of, and P-gp dysfunction in, MBEC4 cells, was aggravated in pericyte co-cultures. We previously reported that treatment with CsA (0.5–10 μM) for 24 h dose-dependently decreased the viability of MBEC4 cells (Kochi *et al.*, 1999). The present study demonstrated that a 12 h-exposure to CsA at concentrations up to 10 μM had no effect on the viability of MBEC4 cells in MBEC4 monolayers and

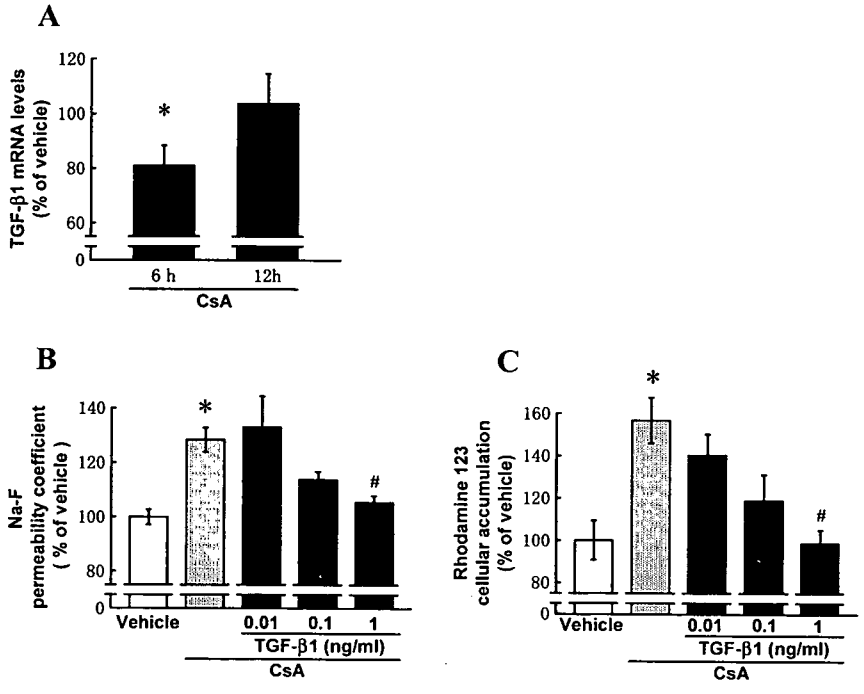

Fig. 2. (A) Effect of CsA (5 μM) on TGF-β1 mRNA expression in brain pericytes at 6 and 12 h after the addition of CsA in pericyte co-cultures. Total RNA of brain pericytes was extracted and subjected to real-time PCR analysis. Fold changes in TGF-β1 mRNA are normalized to GAPDH and compared with each corresponding vehicle treatment. Values are the means ± SEM (n = 3–5). $^*p < 0.05$, significant difference from vehicle. (B) Effect of TGF-β1 on CsA-increased Na-F permeability of MBEC4 cells in pericyte co-cultures. Results are expressed as % of vehicle (vehicle; 3.28 ± 0.22 × 10^{-4} cm/min). Values are the means ± SEM (n = 8–16). $^*p < 0.05$, significant differences from vehicle.$^\#p < 0.05$, significant difference from CsA treatment. (C) Effect of TGF-β1 on CsA-increased rhodamine 123 accumulation of MBEC4 cells in pericyte co-cultures. Results are expressed as % of each corresponding vehicle treatment (vehicle; 1.16 ± 0.24 nmol/mg protein). Values are the means ± SEM (n = 4–12). $^*p < 0.05$, significant differences from vehicle.$^\#p < 0.05$, significant difference from CsA treatment.

pericyte co-cultures. Thus, the exposure time (6 h) and the submaximum concentration (5 μM) of CsA without cytotoxicity were selected here.

The significance of brain pericytes in the regulation of the BBB was suggested by our previous study using a primary culture of rat brain pericytes. We reported that brain pericyte-derived TGF-β1 contributed to the induction and up-regulation of BBB function (Dohgu *et al.*, 2004b, 2005). In the present study, the presence of human brain pericytes decreased the function of tight junctions and increased the function of P-gp, in MBEC4 cells, by about 20%. An interjunctional property of MBEC4 cells was lowered by co-culturing with human brain pericytes, this event being inconsistent with our previous report using a primary culture of rat brain pericytes. The different backgrounds of human brain pericytes commercially supplied and species-different cell type may be compounding factors in this discrepancy

(Lai and Kuo, 2005); however, further studies are required to confirm this. Here, we employed a convenient *in vitro* model with MBEC4 cells and human brain pericytes.

To test whether TGF-β1 production of the brain pericytes participates in the mediation of CsA-induced dysfunction of the BBB, we examined the effect of CsA on the expression of TGF-β1 in brain pericytes. A 6 h-exposure to CsA (5 μM) significantly decreased the levels of TGF-β1 mRNA in brain pericytes in pericyte co-cultures (Fig. 2A). Treatment with TGF-β1 dose-dependently inhibited CsA-induced hyperpermeability and P-gp dysfunction in MBEC4 cells in pericyte co-cultures (Fig. 2B and C). These findings suggest that CsA decreases BBB function by inhibiting TGF-β1 production in the brain pericytes. In pericyte co-cultures, an aggravation of CsA-induced hyperpermeability of MBEC4 cells occurred with a peak at 6 h after the addition of CsA, becoming more moderate at 9–12 h (Fig. 1B). In parallel with these events, TGF-β1 mRNA levels were significantly decreased by a 6 h–exposure to CsA but not by a 12 h-exposure (Fig. 2A), suggesting that CsA-induced hyperpermeability is ameliorated by the compensatory secretion of TGF-β1 from brain pericytes during the later period of CsA exposure. These data further support a critical role of pericyte-derived TGF-β1 in mediating CsA-induced BBB dysfunction.

RT-PCR analysis demonstrated the expression of TGF-β receptor I and II in MBEC4 cells and brain pericytes (Fig. 1A). TGF-β1 mRNA was also detected in brain pericytes (Fig. 2A) and MBEC4 cells (data not shown). Considering these observations, TGF-β is likely to participate in the up-regulation of BBB function through an autocrine and/or paracrine pathway in brain endothelial cells and pericytes. Autoinduction of TGF-β1 is mediated by binding of the transcription factor activator protein-1 (AP-1) complex to homologous elements in two regions of the TGF-β1 promoter (Kim *et al.*, 1990). In this positive autoregulation process, CsA is known to directly inhibit activation of the JunD isoforms in the AP-1 complex responsible for TGF-β signaling in lung fibroblasts (Eickelberg *et al.*, 2001). Calcineurin, a molecular target of CsA, has been shown to be involved in AP-1 activation in immune cells (Pfeuffer *et al.*, 1994; Tsuboi *et al.*, 1994). Based on this evidence, CsA may be interpreted as lowering TGF-β1 expression in brain pericytes due, at least in part, to an inhibition of the AP-1 activation step during TGF-β1 autoinduction. We previously reported that CsA increased NO production in MBEC4 cells (Dohgu *et al.*, 2004a) and elevated levels of NO have been known to reduce TGF-β1 production in the heart (Smith *et al.*, 2005). Therefore, CsA may also act on MBEC4 cells to lower TGF-β1 expression in brain pericytes.

In conclusion, CsA-induced hyperpermeability and P-gp dysfunction of MBEC4 cells were markedly aggravated in co-cultures with brain pericytes. This aggravation appears to occur due to CsA-induced inhibition of TGF-β1 expression in brain pericytes. These findings suggest that an inhibition of brain pericyte-derived TGF-β1 contributes to the occurrence of CsA-induced dysfunction of the BBB, thereby triggering neurotoxicity.

ACKNOWLEDGMENTS

This work was supported, in part, by Grants-in-Aid for Scientific Research ((B) 17390159) from JSPS, Japan and by a Grant-in-Aid for Exploratory Research (17659160) from MEXT, Japan. The authors thank Dr. Mária A. Deli (Institute of Biophysics, Biological Research Centre of the Hungarian Academy of Sciences) for pertinent comments on the manuscript.

REFERENCES

Antonelli-Orlidge, A., Saunders, K. B., Smith, S. R., and D'Amore, P. A. (1989). An activated form of transforming growth factor beta is produced by co-cultures of endothelial cells and pericytes. *Proc. Natl. Acad. Sci. U.S.A.* **86**:4544–4548.

Bradford, M. M. (1976). A rapid and sensitive method for the quantitation of microgram quantities of protein utilizing the principle of protein-dye binding. *Anal. Biochem.* **72**:248–254.

Dehouck, M.P., Jolliet-Riant, P., Bree, F., Fruchart, J. C., Cecchelli, R., and Tillement, J. P. (1992). Drug transfer across the blood-brain barrier: Correlation between *in vitro* and *in vivo* models. *J. Neurochem.* **58**:1790–1797.

Dohgu, S., Yamauchi, A., Nakagawa, S., Takata, F., Kai, M., Egawa, T., Naito, M., Tsuruo, T., Sawada, Y., Niwa, M., and Kataoka, Y. (2004a). Nitric oxide mediates cyclosporine-induced impairment of the blood-brain barrier in co-cultures of mouse brain endothelial cells and rat astrocytes. *Eur. J. Pharmacol.* **505**:51–59.

Dohgu, S., Yamauchi, A., Takata, F., Naito, M., Tsuruo, T., Higuchi, S., Sawada, Y., and Kataoka, Y. (2004b). Transforming growth factor-beta1 upregulates the tight junction and P-glycoprotein of brain microvascular endothelial cells. *Cell. Mol. Neurobiol.* **24**:491–497.

Dohgu, S., Takata, F., Yamauchi, A., Nakagawa, S., Egawa, T., Naito, M., Tsuruo, T., Sawada, Y., Niwa, M., and Kataoka, Y. (2005). Brain pericytes contribute to the induction and up-regulation of blood-brain barrier functions through transforming growth factor-beta production. *Brain Res.* **1038**:208–215.

Eickelberg, O., Pansky, A., Koehler, E., Bihl, M., Tamm, M., Hildebrand, P., Perruchoud, A. P., Kashgarian, M., and Roth, M. (2001). Molecular mechanisms of TGF-(beta) antagonism by interferon (gamma) and cyclosporine A in lung fibroblasts. *FASEB J.* **15**:797–806.

Fontaine, M., Elmquist, W. F., and Miller, D. W. (1996). Use of rhodamine 123 to examine the functional activity of P-glycoprotein in primary cultured brain microvessel endothelial cell monolayers. *Life Sci.* **59**:1521–1531.

Gijtenbeek, J. M., Van Den Bent, M. J., and Vecht, C. J. (1999). Cyclosporine neurotoxicity. *J. Neurol.* **246**:339–346.

Hori, S., Ohtsuki, S., Hosoya, K., Nakashima, E., and Terasaki, T. (2004). A pericyte-derived angiopoietin-1 multimeric complex induces occludin gene expression in brain capillary endothelial cells through Tie-2 activation *in vitro*. *J. Neurochem.* **89**:503–513.

Kahan, B. D. (1989). Cyclosporine. *N. Engl. J. Med.* **321**:1725–1738.

Kim, S. J., Angel, P., Lafyatis, R., Hattori, K., Kim, K. Y., Sporn, M. B., Karin, M., and Roberts, A. B. (1990). Autoinduction of transforming growth factor beta 1 is mediated by the AP-1 complex. *Mol. Cell. Biol.* **10**:1492–1497.

Kochi, S., Takanaga, H., Matsuo, H., Naito, M., Tsuruo, T., and Sawada, Y. (1999). Effect of cyclosporin A or tacrolimus on the function of blood-brain barrier cells. *Eur. J. Pharmacol.* **372**:287–295.

Kochi, S., Takanaga, H., Matsuo, H., Ohtani, H., Naito, M., Tsuruo, T., and Sawada, Y. (2000). Induction of apoptosis in mouse brain capillary endothelial cells by cyclosporin A and tacrolimus. *Life Sci.* **66**:2255–2260.

Lai, C. H., and Kuo, K. H. (2005). The critical component to establish *in vitro* BBB model: Pericyte. *Brain Res. Brain Res. Rev.* **50**:258–265.

Machida, H., Ogawa, K., Funaba, M., Mizutani, T., and Tsujimoto, M. (2000). mRNA expression of type I and type II receptors for activin, transforming growth factor-beta, and bone morphogenetic protein in the murine erythroleukemic cell line, F5-5.fl. *Eur. J. Endocrinol.* **143**:705–710.

Pardridge, W. M. (1999). Blood-brain barrier biology and methodology. *J Neurovirol.* **5**:556–569.